# Wave Propagation and Elasticity in Granular Soils: A Numerical Approach for a Micromechanical Perspective


**Vanessa Magnanimo**

**Abstract** In this work we propose an overview of results about propagation of waves and elasticity in soils over the last 30 years. Remarkably, the chapter attempts to frame and compare contributions from soil mechanics, solid mechanics and physics. In a wide landscape, we focus on the micromechanical approach to the topic. Numerical simulations, based on the Discrete Element Method, have revealed the outmost role of the microstructure in characterising the elastic behaviour of granular soils. Following this evidence, microstructure-based continuum models have been developed and are discussed here, starting from the classical Effective Medium Theory. Finally, the chapter describes how micromechanical models can be extended to the case of immersed granular soils, and compares the new model with experiments on sand soils in a wide range of saturation degrees.

**Keywords** Granular materials · Wave propagation · Elasticity · Micromechanics · Discrete Element Method

## 1 Introduction: Overview

For many geotechnical structures under working loads, the deformations are small. The regime of deformation where the behaviour of soils can be considered linear elastic is infinitesimal, with nonlinear and irreversible effects present already at small strains. Nevertheless, characterisation of the stiffness of soils is of outmost importance, as it provides an anchor on which to attach the subsequent stress-strain response [6, 39].

V. Magnanimo (✉)
MultiScale Mechancs (MSM), TFE, Mesa+, University of Twente, Enschede, Netherlands

Construction Management & Engineering (CME), University of Twente, Enschede, Netherlands
e-mail: v.magnanimo@utwente.nl, https://www.utwente.nl



P. Giovine et al. (eds.), *Views on Microstructures in Granular Materials*, Advances in Mechanics and Mathematics 44, https://doi.org/10.1007/978-3-030-49267-0_6

Despite the long-standing debate across the geomechanical, mechanical and physics communities, basic features of the physics of granular elasticity are currently unresolved, like the definition of a proper set of state variables to characterise the effective moduli. In early studies, macroscopic variables measurable in laboratory experiments were thought to be sufficient. Based on those information, many empirical relations have been proposed, where the elastic moduli are functions of pressure and void ratio, e.g., [4, 16, 17, 46]. However, such formulations miss a first order mechanical interpretation and coefficients have to be back-calculated case by case from experiments, based on the specific material and stress path. Moreover, experimental evidences [7, 13, 27, 44], along with many numerical studies [2, 35], show that stress and volume fraction are not sufficient to characterise granular elasticity.

On the other hand, conventional approaches in the framework of solid-state elasticity [31] consider a uniform strain at all scales, with the displacement field of the grains following the macroscopic deformation (affine approximation). These Effective Medium Theories (EMT) developed by Digby and Walton [10, 52] in the 1980s are the first, simplest attempt for a micromechanical approach to the elasticity of granular soils. EMT predicts the moduli of an isotropic granular material in terms of the external pressure, the void ratio and average coordination number ($p_0$, $e$, $Z$). In particular, the pressure dependency is $G \sim K \sim p_0^{1/3}$, a direct consequence of the Hertz interaction between particles. However, such scaling is not recovered in experiments and previous works (see [15] for a review) raise serious questions about the validity of these generally accepted theoretical elastic formulations.

Empirical relations coming from experiments and micromechanical EMT equations show many similarities and the two approaches can fruitfully inform each other. Following one of the paths suggested already in [15] and further developed in [33, 35], this chapter shows that when the evolution of the microstructure is properly modelled, the set of state variables to describe granular elasticity is complete, and experiments follow the trend predicted by the model. This is obtained with the aid of Discrete Element Simulations (DEM) that uniquely allow to monitor the kinematics at the microscale and establish a link it with the macroscale.

However, the EMT framework still largely overpredicts the elastic moduli of loose samples, especially when shear is involved. The difficulty in describing theoretically the shear modulus is due to the complex relaxation of the particles as related to the structural disorder in the packing [35]. Sophisticated theories in which collective fluctuations and relaxation of the particles are explicitly accounted for are needed to recover quantitative agreement. Here we briefly illustrate the mechanics beyond these theories and compare the results with numerical simulations.

This chapter has the ambition to link the work on wave propagations and granular elasticity from different scientific communities. The work offers a wide perspective, even if non-comprehensive, to elucidate on the microscopic origin of macroscopic phenomena related to elasticity and wave propagation in particulate media. For the sake of simplicity, here we focus on of an isotropic materials to illustrate traditional models and new findings.

Additionally we extend our study, by illustrating a recent work where the simple EMT has been successfully combined with a geomechanical framework to provide a micromechanical model for unsaturated sand [42]. The model is able to interpret experimental results, and to elucidate the mechanisms underlying different patterns of the shear modulus in unsaturated materials observed in the literature.

The chapter is organised as follows: in Sect. 2, the classical relations between wave velocity and elastic moduli in a solid are derived; Sect. 3 introduces the specific features of waves in granular materials as observed at macroscopic level and the empirical models based on them; Sect. 4 describes the micromechanical approach based on the Effective Medium Theory and Sect. 5 compares the predictions of EMT theory with DEM simulations; in Sect. 6, advanced micromechanical models accounting for fluctuations are introduced and compared with DEM data. Finally in Sect. 7, the micromechanical approach is extended to describe wave propagation in unsaturated soils.

## 2 Waves in Solids: The Duality Between Waves and Elasticity

A wave is an elastic perturbation that propagates between two points through a body (volume waves) or on the surface (surface waves) without material displacement [3]. In the case of volume waves the acoustic-elastic effect is related to the change in the wave velocity of small amplitude waves due to the stress state of the body. Differently from liquids, in a solid material three acoustic polarisations exist, more specifically a longitudinal and two transversal branches. In the present section, we will derive the relations between the elastic characteristics and the velocities of acoustic waves, in the longitudinal and transversal directions.

Let us consider a three-dimensional body with density $\rho$, homogeneous, isotropic and elastic. The stress change due to the propagation of the wave in the body is given by the Newton's second law applied to the volume element $\rho dV$ [9]:

$$\frac{\partial \sigma_{ij}}{\partial x_j} = \rho \ddot{u}_i, \tag{1}$$

with $\sigma_{ij}$ stress and $u_i$ displacement of the volume element in directions $i, j = 1, 2, 3$. On the other hand, the constitutive relation for the elastic body holds that relates the stress tensor to the strain $\epsilon_{ij}$ via the stiffness tensor $C_{ijkl}$

$$\dot{\sigma}_{ij} = C_{ijkl}\dot{\epsilon}_{kl}. \tag{2}$$

In the isotropic case, Eq. (2) becomes (Lamé equation)

$$\dot{\sigma}_{ij} = \lambda \Theta \delta_{ij} + 2G\epsilon_{ij}, \tag{3}$$

where $\Theta = \sum_{i=1}^{3} \epsilon_{ii}$, $G$ and $\lambda$ are the shear modulus and Lamé coefficient, respectively, and the incremental strain tensor is given by

$$\epsilon_{ij} = \frac{1}{2}\left(\frac{\partial u_i}{\partial x_j} + \frac{\partial u_j}{\partial x_i}\right). \tag{4}$$

The bulk modulus is related to the previous quantities as $K = \lambda + 2/3G$.

Using Eqs. (3–4) in Eq. (1) and the relation $\Theta = \dfrac{\partial u_i}{\partial x_i}$, the equation of motion becomes

$$\rho\frac{\partial^2 u_i}{\partial t^2} = \frac{\partial}{\partial x_j}\left(\lambda\frac{\partial u_i}{\partial x_i}\right) + G\frac{\partial^2 u_i}{\partial x_j^2} + G\frac{\partial}{\partial x_i}\left(\frac{\partial u_i}{\partial x_j}\right). \tag{5}$$

From Helmholtz decomposition, the displacement vector $\boldsymbol{u}$ can be written in terms of a scalar potential $\phi$ and a vector potential $\boldsymbol{\psi}$ as

$$\boldsymbol{u} = \nabla\phi + \nabla \times \boldsymbol{\psi}, \tag{6}$$

with

$$\nabla \times (\nabla\phi) = \mathbf{0} \qquad \text{and} \qquad \nabla \cdot (\nabla \times \boldsymbol{\psi}) = 0, \tag{7}$$

due to the properties of divergence and curl. Note the tensorial notation has been introduced here for the sake of brevity.

By using the decomposition in Eq. (6), Eq. (5) becomes

$$\nabla\left[\rho\frac{\partial^2\phi}{\partial t^2} - \left(\lambda + \frac{4}{3}G\right)\nabla^2\phi\right] + \nabla \times \left[\rho\frac{\partial^2\boldsymbol{\psi}}{\partial t^2} - G\nabla^2\boldsymbol{\psi}\right] = \mathbf{0}. \tag{8}$$

Equation (8) is known as the wave equation and predicts longitudinal and transversal modes of propagation. The first term depends only on $\phi$ and is related to the propagation of waves in the longitudinal direction, while the second term depends on the vector potential $\boldsymbol{\psi}$ and is associated with transversal waves. Both terms must be separately zero to satisfy Eq. (8), that is, the two propagation modes, longitudinal and transversal, are independent.

Let us define the longitudinal and shear components of the displacement as

$$\boldsymbol{u}_P = \nabla\phi \qquad \text{and} \qquad \boldsymbol{u}_S = \nabla \times \boldsymbol{\psi}. \tag{9}$$

The combination of Eqs. (7) and (9) leads to constrains for $\boldsymbol{u}_P$ and $\boldsymbol{u}_S$. Because of $\nabla \times \boldsymbol{u}_P = \mathbf{0}$, there are no angular displacements and rotations associated with $\boldsymbol{u}_P(\phi)$, being this a characteristic of longitudinal waves. Similarly, $\nabla \cdot \boldsymbol{u}_S = 0$

assures that volume changes associated with $\boldsymbol{u}_S(\boldsymbol{\psi})$ are forbidden, as expected for transversal waves.

Finally, Eq. (8) results in the following two equations:

$$\frac{\partial^2 \boldsymbol{u}_P}{\partial t^2} = V_P^2 \nabla^2 \boldsymbol{u}_P \qquad \text{and} \qquad \frac{\partial^2 \boldsymbol{u}_S}{\partial t^2} = V_S^2 \nabla^2 \boldsymbol{u}_S, \tag{10}$$

where

$$V_P = \sqrt{\frac{(\lambda + 4/3G)}{\rho}} \qquad \text{and} \qquad V_S = \sqrt{\frac{G}{\rho}} \tag{11}$$

are the velocities of longitudinal and transversal waves in an isotropic elastic body.

From Eq. (11), we can immediately draw some interesting conclusions: (1) the propagation velocity increases with the stiffness of the material and decreases with its mass density (inertia), these characteristics being constants in a given solid body; (2) the velocity of transversal waves is smaller than the velocity of longitudinal waves, given the relative values of the moduli.

## 3 Waves in Granular Media

We move now our attention from solid to particulate materials. In this section we will highlight the most relevant features characteristic of wave propagation in granular materials.

When the wavelength is significantly longer than the internal scales of the material, such as particle or cluster size, the propagation velocity can be defined for the equivalent continuum, that is, Eqs. (11), where the elastic moduli and mass density refer to the bulk medium. Differently, for high frequencies and short wavelengths, the continuum assumption does not hold, due to the heterogeneity of the material at small scale and forces fluctuation [50]. With increasing frequencies, features related to the multiscale nature of soils become dominant, e.g., dispersion and frequency filtering. These aspects are beyond the scope of this work and in the next sections the focus will be on the long wave length limit.

Other than frequency, also amplitude is an important factor to take into account. The propagation of elastic waves is, by definition, a small perturbation phenomenon that does not alter the fabric or cause permanent (plastic) effects. This condition must be guaranteed for the continuum analogy to hold. This is shown by the degradation curve obtained in the resonant column device that provides values of the elastic shear stiffness $G$ for increasing amplitude of the shear strain. A typical output of the resonant column experiment is given in Fig. 1. The figure shows that the response of granular materials is nonlinear and inelastic even at extremely small strains. The region of stress or strain in which granular materials can be described as truly elastic, producing an entirely recoverable response to

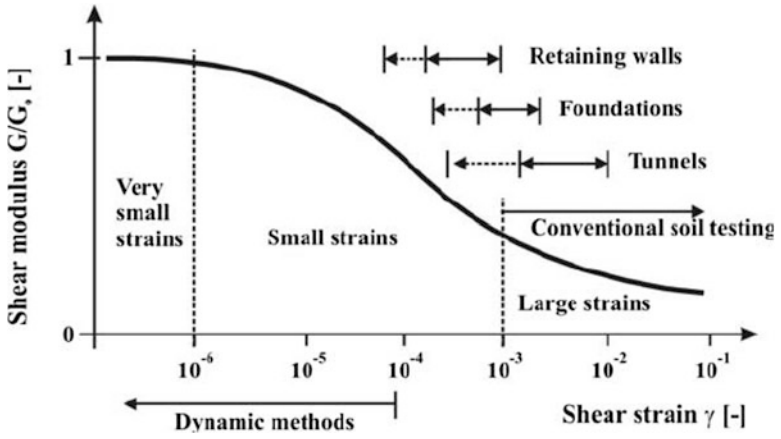


**Fig. 1** Degradation curve for $G$ with indication of typical soil tests and geotechnical applications per strain regime [34]

perturbations, the so-called small-strain stiffness $G_{max}$, is very small, corresponding to shear strains of the order of $10^{-6}$. In turn, the size of the elastic, reversible regime depends on material characteristics, stress state, anisotropy: the elastic range increases with increasing asperities (particle friction) and pressure, but decreases with increasing anisotropy. Strain-amplitude-dependent moduli are not addressed further here, although its importance is widely recognised. In the following, all references will be to the small-strain shear modulus $G_{max}$ and we will use simply $G$ for it, unless otherwise stated.

If both conditions, long wavelength and small amplitude, are fulfilled, wave measurements (obtained, e.g., via wave transducers) can be used to infer elastic moduli and vice versa.

## *3.1 Macroscale Observations: Pressure-Dependent Elasticity*

Several authors have carried on experiments to assess the influence of material characteristics and initial conditions on the elastic/wave properties of natural and synthetic granular materials, see, for example, [7, 17, 30] for experiments on sand in the resonant column device or [11, 29] for wave experiments on sand and glass beads. At the macroscopic level, all these studies lead to a similar conclusion that the initial soil stiffness is a nonlinear function of the stress, specifically the mean effective stress. Based on experiments, empirical expressions have been proposed for the shear stiffness of soils under isotropic conditions (e.g., [4, 16, 17, 30]):

$$G = Af(e)p_0^{\alpha} \qquad \text{hence} \qquad V_s = Af(e)p_0^{\alpha/2}, \tag{12}$$

where $A$ and $\alpha$ are experimentally determined constants, $p_0$ is the hydrostatic pressure and $f(e)$ is a function that describes the effect of void ratio $e$ again obtained empirically, e.g., [16]:

$$f(e) = \frac{(2.97 - e)^2}{(1 + e)}. \tag{13}$$

In Eq. (12) the exponent $\alpha$ and the factor $A$ are assumed to be constants, related to the material characteristics and independent of the stress level. Differently from $f(e)$, there is no common interpretation for $\alpha$ and $A$ and they must be retrieved case by case from experiments. Hardin [16, 17] has reported values of $\alpha$ around 0.25 for sands. The same value was confirmed in [30]. Domenico in [11] conducted experiments on dry/unsaturated glass beads and sands. He obtained a very similar expression to Eq. (12) with the exponent depending on the saturation degree. Values of $\alpha$ close to those reported by Hardin were found in the case of dry materials, with negligible differences between rounded sand and glass beads.

While the majority of these studies are restricted to isotropic loading conditions, in their initial work, Hardin and Black [16] suggested that Eq. (12) can be extended to anisotropic soils. Later on, modifications (see, for example, [4, 46]) have led to a generalised expression of the form:

$$G = A f(e) p_0^{1-\beta_i-\beta_j} \sigma_i^{\beta_i} \sigma_j^{\beta_j}, \tag{14}$$

where the directions $i$ and $j$ of polarisation and propagation coincide with the principal axes of stress and of anisotropy of the material [39]. The expression suggests that the stiffness depends on the principal stresses in the directions of polarisation and propagation. A wide range of values has been reported for $\beta_i$ and $\beta_j$ depending on the specific stress path.

Thus, extensive experimental evidences and theoretical studies support the choice of a power function to relate stiffness and stress. What is still missing is the physical interpretation of the parameters $A$ and $\alpha$ in Eq. (12). An intriguing interpretation associates those to the structure of the granular soil, i.e., the fabric. Among others, the authors in [7] have related the dynamic shear modulus of glass beads in resonant column monotonic/cyclic tests to the fabric, as the sample was sheared in various directions with constant mean stress. Santamarina [47] has observed different scaling of the wave velocities at low/high stress and identified a transition between two regimes with varying and constant fabric, respectively. More recently, the authors in [13] have used bender elements to underline the effect of (inherent and induced) anisotropy on the elastic stiffness of sand under triaxial conditions. In these experiments features of the elastic behaviour of the material are linked to the internal structure. From there, the relation between the parameters in Eq. (12) and the fabric can be indirectly inferred.

In the next section we will use a different approach and derive the elastic properties of the bulk starting from the grain scale. Finally we will compare the

results with the empirical relations presented above. When general expressions are confirmed, wave velocities and stiffness experiments can be used as indirect measurement of the internal structure of the granular medium or to monitor fabric changes induced by loading.

## 4 Micromechanics

The experiments referred to in Sect. 3.1 are examples of approaches that rely on macro measurements. On the other hand, the state of the granular medium at the micromechanical level is defined by the distribution of contacts, forces and orientations. In turn, it is possible to describe the macroscopic stiffness of the granular medium in terms of its micromechanical characteristics.

In this section, we will derive the expression of the stiffness tensor for an isotropic assembly of identical spheres, starting from the grains interaction. Then we will compare the expression with Eq. (12) and show how micromechanics is able to explain the empirical coefficients obtained from experiments.

### *4.1 Interaction at the Grain Level*

**Kinematics** We consider a dense aggregate of $N_B$ identical, frictional elastic spheres with diameter $d$, isotropically compressed. The contact point $c$ between two contacting particles $A$ and $B$ is identified by the unit vector $n_i$ along the line that joins the centres of the two spheres. The unit vector $t_i$ belongs to the plane tangent to the spheres in $c$. The kinematics of the pair $A - B$ is given by the incremental relative displacement between the centres

$$\dot{u}_i^{(BA)} = \dot{X}_i^B - \dot{X}_i^A - \frac{1}{2}\epsilon_{ijk}(\dot{\theta}_j^B - \dot{\theta}_j^A)n_k, \tag{15}$$

where $\dot{X}_i^A, \dot{X}_i^B$ and $\dot{\theta}_i^A, \dot{\theta}_i^B$ are the increments in the centres translation and rotations, respectively, and $\epsilon_{ijk}$ is the permutation tensor. For the sake of simplicity, we will assume in the following that the rotational velocities are infinitesimally small. Thus $\dot{u}_i^{(BA)}$ can be expressed in terms of the normal component $\dot{\delta}_i$ and $\dot{s}_i$ with

$$\dot{\delta}_i = \dot{\delta} n_i = (\dot{X}_k^B - \dot{X}_k^A)n_k n_i \tag{16}$$

and tangential component

$$\dot{s}_i = (\dot{X}_i^B - \dot{X}_i^A) - \dot{\delta} n_i. \tag{17}$$

We also introduce here the branch vector $l_i^c$ that connects the centres of $A$ and $B$ interacting at $c$ and relates to the particle diameter as

$$l_i^c = (X_i^B - X_i^A) = dn_i. \tag{18}$$

**Contact Force** Contacting particles interact by means of contact forces. We denote by $f_i^c$ the $i$-th component of the force exerted on particle $A$ by particle $B$. Since we are interested in the incremental response of the aggregate, we will refer to the incremental force $\dot{f}_i^c$. In this case, when deformations are small, the incremental response is elastic, proportional to the relative displacement in both normal and tangential directions. If we denote by $K_N$ and $K_T$ the normal and tangential components of the stiffness the constitutive law at the contact is

$$\dot{f}_i^c = K_N \dot{\delta} n_i + K_T \dot{s}_i. \tag{19}$$

$K_N$ and $K_T$ are constant values if a linear contact model is considered. When Hertz contact interaction is assumed [18], $K_N$ and $K_T$ are functions of the normal component $\delta$ of the relative displacement, the diameter $d$ of the spheres, and their material properties

$$K_N = \frac{G_g d^{1/2}}{1-\nu} \delta^{1/2} \tag{20}$$

and

$$K_T = \frac{2G_g d^{1/2}}{2-\nu} \delta^{1/2}, \tag{21}$$

where $G_g$ and $\nu$ are the shear modulus and Poisson's ratio of the individual particle.

**Incremental Stress** At the macroscale the relevant quantities are the incremental stress tensor $\dot{\sigma}_{ij}$ and the strain tensor $\dot{\epsilon}_{ij}$. Given the incremental force, the incremental stress tensor is determined by the particle arrangement as [26]

$$\dot{\sigma}_{ij} = \frac{1}{V} \sum_{\theta} \sum_{c \in N^c(\theta)} l_i^c \dot{f}_j^c, \tag{22}$$

that is, the average on the volume $V$ of the Cauchy's stress [31], with $N^c$ total number of contacts. The equation emphasises the dependence of the stress on the average of forces on equally oriented contacts. In the case of a regular array, the values of $l_i^c$ and $\dot{f}_i^c$ are known for each contact and the components of $\dot{\sigma}_{ij}$ can be easily determined. For a random isotropic aggregate of particles of the number of contacts for each orientation $\theta$ is the same, and can be characterised by the scalar coordination number, i.e., the average number of contacts in the sample

$Z = 2N^c/N_B$, with $N_B$ number of particles in $V$. Then, the incremental stress simplifies to the form

$$\dot{\sigma}_{ij} = \frac{Z}{V}\left\langle l_i^c \dot{f}_j^c \right\rangle. \tag{23}$$

## 4.2 Theoretical Modelling: The Effective Medium Theory

The Effective Medium Theory (EMT) assumes that the incremental displacement of each point $X$ in the (discrete) body is given by the applied average strain $\dot{\epsilon}_{ij}$ [10, 52]. Following this hypothesis, the relative displacement between contacting particles is

$$\dot{u}_h^{(BA)} = \dot{X}_h^B - \dot{X}_h^A = \dot{\epsilon}_{hk} l_k^c = \dot{\epsilon}_{hk} d n_k, \tag{24}$$

thus, the normal and tangential components of the incremental displacement become

$$\dot{\delta} = d\dot{\epsilon}_{hk} n_h n_k \qquad \text{and} \qquad \dot{s}_j = \dot{\epsilon}_{jk} d n_k - d\dot{\epsilon}_{hk} n_h n_k n_j. \tag{25}$$

Using Eqs. (18) and (25) in Eq. (19) the incremental stress can be rewritten as

$$\dot{\sigma}_{ij} = \frac{d^2}{V} \sum_\theta \sum_{c \in N^c(\theta)} \left[ \left\langle K_N \dot{\epsilon}_{hk} n_h n_k n_i n_j \right\rangle + \left\langle K_T \dot{\epsilon}_{jk} n_i n_k \right\rangle - \left\langle K_T \dot{\epsilon}_{hk} n_h n_k n_i n_j \right\rangle \right]. \tag{26}$$

Using Eq. (2) in its incremental form, after some further algebra, we find the following solution for the stiffness tensor:

$$\begin{aligned} C_{ijkh} &= \frac{\dot{\sigma}_{ij}}{\dot{\epsilon}_{hk}} = \\ &= \frac{d^2}{V} \sum_\theta \sum_{c \in N^c(\theta)} \left[ \left\langle (K_N - K_T) n_h n_k n_i n_j \right\rangle \right] \\ &+ \frac{d^2}{V} \sum_\theta \sum_{c \in N^c(\theta)} \frac{1}{4} \left[ \left\langle K_T \delta_{jh} n_i n_k \right\rangle + \left\langle K_T \delta_{ik} n_j n_h \right\rangle + \left\langle K_T \delta_{ih} n_j n_k \right\rangle + \left\langle K_T \delta_{jk} n_i n_h \right\rangle \right]. \end{aligned} \tag{27}$$

In the case of a regular array of particles the values of $n_i$ are known exactly, and the volume fraction and number of contacts are constant values in the unit cell of spheres. That is, the stiffness assumes simplified forms, for example, in the case of Face Centred Cubic (FCC) packing that will be treated in Sect. 5.1 or Square Cubic (SC) packing in Sect. 7.1.

For a random assembly of spheres, we can use the simplified Eq. (23) to obtain

$$C_{ijkh} = \frac{d^2 Z}{V}\left[\left\langle (K_N - K_T) n_h n_k n_i n_j \right\rangle\right] \tag{28}$$
$$+ \frac{d^2 Z}{V}\frac{1}{4}\left[\left\langle K_T \delta_{jh} n_i n_k \right\rangle + \left\langle K_T \delta_{ik} n_j n_h \right\rangle + \left\langle K_T \delta_{ih} n_j n_k \right\rangle + \left\langle K_T \delta_{jk} n_i n_h \right\rangle\right].$$

Finally, when Hertzian contacts are considered, subjected to an initial isotropic compression, the relative normal displacement $\delta$ is related with the hydrostatic pressure $p_0 = 1/3\mathrm{tr}(\sigma_{ij})$ as

$$\delta = d\left[\frac{3\pi}{2}\frac{(1-\nu)p_0}{G_g Z \phi}\right]^{2/3}, \tag{29}$$

where $\phi = \pi d^3 N_B / 6V$ is the volume fraction. Equation (29) gives $K_N$ and $K_T$ in Eqs. (20) and (21) as functions of the state variables of the initial, reference state, $p_0, \phi, Z$ [20, 35]. The average strain assumption results in the following expression for the shear and bulk moduli $G$ and $K$:

$$G = \frac{5 - 3\nu}{20}\phi^{2/3} Z^{2/3} p_0^{1/3}\left[12\left(\frac{G_g}{\pi(1-\nu)}\right)^2\right]^{1/3} \tag{30}$$

and

$$K = \frac{1}{3}\phi^{2/3} Z^{2/3} p_0^{1/3}\left[\frac{3}{2}\left(\frac{G_g}{\pi(1-\nu)}\right)^2\right]^{1/3}. \tag{31}$$

The relations above show that the elastic properties of the granular material depend only on the material characteristics and the values of $p_0, \phi, Z$ in the reference state. They are not related explicitly to the previous history of the sample, other than through the values that such history assigns to the state variables.

We want now to compare the micromechanical expressions (Eq. (30)) for $G$ with the empirical relations proposed by Hardin and other investigators (Eq. (12)). By adopting equations of the form (Eq. (12)) and given the relation between volume fraction and void ratio $e$

$$\phi = \frac{1 + 2e}{1 + e},$$

the parallelism appears to be remarkable. A first major difference involves the exponent of $p_0$. In EMT the exponent is a constant value that relates directly to the nature of the contact interaction, e.g., $\alpha = 1/3$ for Hertzian contacts as shown above. The exponent $\alpha$ in Eq. (12) is a fitting parameter, back-calculated from

experimental data. However, the experimental measurement of $\alpha$ requires data at different pressure values that involve changes in the number of contacts. Information on such evolution are not accessible from macroscopic observations that (usually) only provide $\phi$ and $p_0$, while it is well known that imperceptible changes in $\phi$ may lead to big changes in $Z$ [48]. Hence, $\alpha$ represents not only the nature of the contact stiffness but also the effect of changes in contacts [48]. If this circumstance is assumed and two different exponents are derived for pressure and coordination number, the Hertzian scaling reconciles with the experimental evidence. This is in the spirit of EMT that proposes $\phi$, $p_0$ and $Z$ as independent quantities.

In the following, we will introduce a numerical procedure to simulate wave propagation in granular materials. Based on the micromechanical insights from the simulations, we can improve the understanding about the dependence of the elastic moduli on the individual state variables, and the cross correlations between them.

## 5 Discrete Element Simulations

The Discrete Element Method (DEM) as introduced by Cundall and Strack [8] is a unique tool for direct exploration of the microstructure in a granular material. In the DEM method, the deformation of the assemblies is computed by numerically integrating in time the equations of motion of all particles, and the results can be employed to analyse the actual state of the material (at both macro- and microscale) and deformation mechanisms.

If the sum of all forces, $\sum_{c \in N^c(A)} f_i{}^c(A)$, acting on particle $A$, either from other particles, from boundaries or from external forces, is known, the problem is reduced to the integration of Newton's equations of motion for the translational and rotational degrees of freedom:

$$m^{(A)}\ddot{x}_i^{(A)} = \sum_{c \in N^c(A)} f_i^c(A) \qquad \text{and} \qquad I^{(A)}\ddot{\theta}_i^{(A)} = \sum M_i(A), \tag{32}$$

with the mass $m^{(A)}$ of particle $(A)$, its position $x_i^{(A)}$, its moment of inertia $I^{(A)}$, its angular velocity $w_i^{(A)} = \dot{\theta}_i^{(A)}$ and the total torque $\sum M_i(A)$. That is, the interaction between particles is given by a non-central contact force in which the normal component follows the expressions introduced in Sect. 4.1. In the tangential direction a bilinear force-displacement relationship is often used, elastic with Coulomb friction threshold. The micromechanical definition of stress given by Eq. (23) holds for a DEM assembly. Periodic boundary conditions are usually employed to reduce boundary effects, and gravity is neglected.

When looking at the microstructure, the coordination number $Z$ is a quantity of interest as it characterises the contact arrangement. The simplest definition of the coordination number has been introduced in the previous section. However,

numerical simulations have revealed that at any time, during compression, there are some particles with no contacts and some particles with only one contact. Those particles do not meet the condition of equilibrium; hence, they are unloaded and do not contribute to the transmission of stress through sample. The mechanical coordination number was introduced in [51]:

$$Z = \frac{2N^c - N_1}{N_B - N_0 - N_1}, \tag{33}$$

where $N_1$ and $N_0$ are the number of particles with only one or no contacts, respectively. When discussing DEM results, we will always refer to the mechanical coordination number, if not stated otherwise. In the case of isotropic systems the scalar quantity $Z$ can be used as main descriptor of the microstructure for all samples. When anisotropic systems are considered, the fabric tensor, able to describe the orientation of the contact network, must be introduced, along with the coordination number.

In the following we will use DEM simulations to study the propagation of waves and elasticity in granular materials. We will analyse two cases, a regular structured array and a random, isotropic aggregate of spheres. In the first case (Sect. 5.1) waves are agitated by perturbation, at the one end of the granular packing, this resembling wave transducers tests [29]. For the random system, the elastic moduli are calculated directly (Sect. 5.2) via an overall strain perturbation applied to the particles. In this way, two numerical approaches are discussed, both suitable either for regular or random packings and leading to identical results for long wavelength and small-strain amplitude (as discussed in Sect. 3). DEM simulations offer direct access to microscale information, allow to verify the micromechanical assumptions proposed by the EMT and, in turn, formulate new, more sophisticated micromechanical models.

## *5.1 DEM Simulations of Structured Arrays of Particles*

It is expected that a regular, structured packing of identical particles moves because of affine motion only and then follows the prediction of the Effective Medium Theory. Several authors have worked out this assumption. Among others, in [38] the authors have performed wave propagation DEM simulations on monodisperse, structured (crystal) packings and compared results with predictions from EMT theory. The configuration considered there is a dense, static, FCC packing, see Fig. 2. In this configuration, a unit cell (cuboid) has a volume $V_u = \sqrt{2}d^3$ and contains two particles with volume $2V_A = (\pi/3)d^3$ such that the volume fraction is $\phi = 2V_p/V_u = \pi/(3\sqrt{2}) \approx 0.74$. Each particle has four contacts inside each square-layer, and eight with particles in both neighbouring layers, corresponding to a coordination number $Z = 12$. Being the packing regular and homogeneous, the system is in a static equilibrium. A small overlap, i.e., contact deformation in

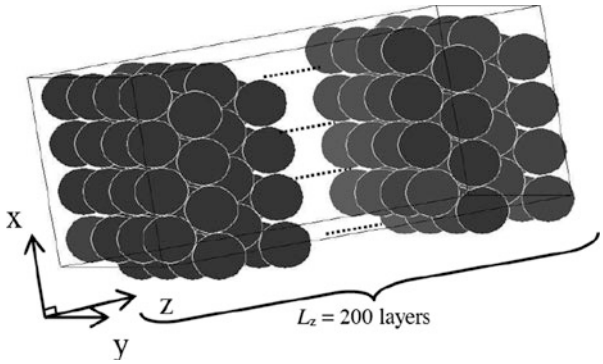


**Fig. 2** Snapshot of a typical body centred cuboid packing from [38]

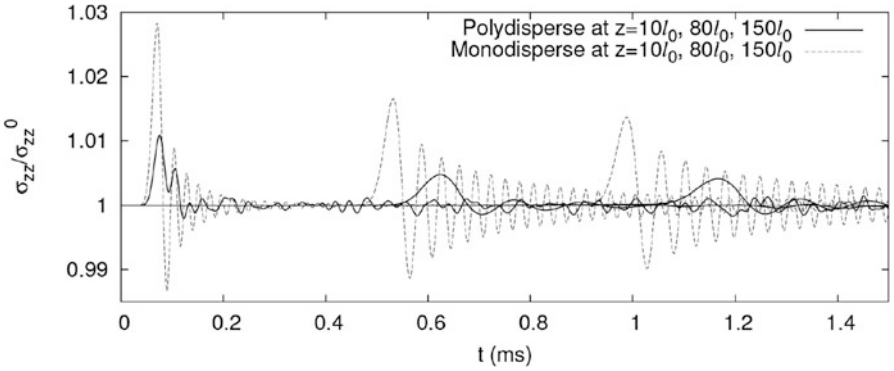


**Fig. 3** Normal stress ($\sigma_{zz}$) scaled by the equilibrium stress ($\sigma_{zz}^0$) as function of time at different positions $z/l_0 = 10$, 80 and 150, with the distance from the source, $z$, and the layer distance $l_0$ [38]

normal direction, between all particle is applied, much smaller than the particle diameter, $\delta/d \approx 10^{-3}$. The applied overlap defines the stress state of the packing $p_0$. Waves are excited by applying a small perturbation at one side of the system, i.e., by shifting a layer of particles. Compressive (P) and shear (S) modes can be triggered by directing the perturbation parallel or perpendicular to the wave propagation direction, respectively. Perturbations of small amplitude with respect to the typical overlap are chosen, $\Delta z/\delta = 10^{-1}$, such that the structure does not change during the simulations. Since the system is made of layers, it is possible to "record" the pulse at each layer as a function of time. As an example, Fig. 3 shows the output of a numerical experiment where a plan compressive P-wave is created and propagated in $z$-direction. The scaled normal stress is plotted versus time at different positions along the wave propagation direction. The figure nicely resembles the travel of the wave as seen in experiments. By looking at the behaviour of stress over time in a given layer, it is possible to detect the arrival time. Since the distance $L$ between

the source layer and the arrival layer is known, the velocity can then be calculated as $V_P = L/t_a$, with $t_a$ arrival time. The simulation results can be compared with the wave speed predicted from Eq. (11) where Eq. (27) provides the elastic moduli. The assumption of a constant stiffness, which holds for small deformations and large wavelength limit, is respected in this case. A very good agreement is obtained between theory and simulations, where the discrepancy is only about 3%. cient, which is kept constant to = 0:5 and kt ness for which we performed a parameter study with the following erences of static and dynamic friction cients, or di erent magnitudes of , relevant here (data not shown). Of course by cially low value for (= 0:001), see [17], sliding contacts occur andThe ness tensor and using the simulation data in order to get the

Later on, the authors check the EMT for a slightly different system, by assigning a size distribution to the particles ($\Delta a$ of the order of the overlap $\delta$). As soon as polydispersity is introduced, and already for small values, the induced disorder in the micromechanical equilibrium forces particles to a kinematics more complex than the affine motion. Note that the coordination number of the relaxed is $Z = 9.975$. This represents a loss of 17% of the contacts as compared to the ordered system ($Z = 12$), but stays constant during propagation of waves. In this nonlinear context, the EMT immediately fails, with discrepancies up to 9% as shown in Fig. 4.

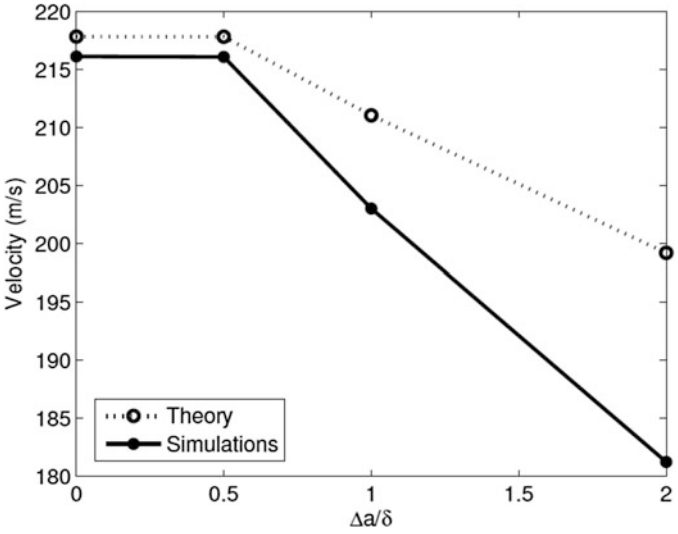


**Fig. 4** P-wave velocities as function of polydispersity: comparison between simulations and EMT theory [38]

## 5.2 DEM Simulations of Random Aggregates

When moving from the regular packing of spheres, to random aggregates, the deviation from the predictions of the Effective Medium Theory becomes more dramatic. In particular, one would expect that an aggregate of random spheres in contact scales with pressure following the relation in Eqs. (30)–(31), i.e., the packing behaves as a collection of Hertzian springs. However, experimentally it is known that the bulk modulus $K$ and shear modulus $G$ of a granular assembly increase with pressure $p_0$ faster than the law predicted by EMT based on Hertz-Mindlin contact forces:

$$K(p_0) \propto p^{1/3} \qquad \text{and} \qquad G(p_0) \propto p^{1/3}.$$

Rather, numerous studies show values dependence of incremental elastic moduli on pressure $p_0$ as $p_0^{1/2}$, as already mentioned in Sect. 3.1. In [15], Goddard presents a comprehensive analysis comparing two alternative mechanisms for the anomalous pressure scaling: (1) the breakdown of the Hertz-Mindlin force law at the level of individual grains due to sharp asphericities at the contact departures; (2) the variation of the number of contacts during pressure increase. He shows that both mechanisms result in a $p_0^{1/2}$ pressure scaling at low pressure and both exhibit a high-pressure transition to $p_0^{1/3}$ scaling at a characteristic transition pressure value.

While Goddard privileges the first hypothesis, the study proposed in [35] supports the second hypothesis with the aid of DEM simulations. In this study, the elastic moduli of isotropic monodisperse packings are calculated directly, by applying an incremental strain to the sample and then measuring the resulting incremental stress. The friction coefficient is set on a very high value to prevent sliding among grains. When a shear strain, $\Delta\epsilon_{12}$ is applied and the change in stress $\sigma_{12}$ is measured after relaxation, the shear modulus is recovered as $G = \Delta\sigma_{12}/\Delta\epsilon_{12}$. Similarly, an incremental isotropic strain, $\Delta v = \Delta\epsilon_{11} + \Delta\epsilon_{22} + \Delta\epsilon_{33}$, is applied to measure $K$. Other than the anomalous scaling with pressure, the shear modulus measured in the simulation is approximately 60% lower than that predicted by EMT (with discrepancies even more dramatic for frictionless spheres), while the difference in the measured and predicted bulk modulus is negligible. The authors in [35] conclude that EMT can describe the scaling between moduli and pressure observed in experiments if the increasing number of grain-grain contacts with $p_0$ is considered. The authors propose an empirical relation for the evolution of the coordination number with pressure of the form

$$\langle Z(p) \rangle = 6 + \left( \frac{p_0}{0.06\,\text{MPa}} \right)^{1/3}. \tag{34}$$

Once this is properly included in the EMT, a good agreement between theory and simulations is recovered.

In the same years, an independent work by Aloufi and Santamarina [47] suggested a similar micromechanical interpretation to their wave transducer experiments on Houston sand. The authors observe a transition in the behaviour of shear wave with pressure and suggest the existence of two regimes: "plastic", i.e., where contacts change, for $p_0 < \overline{p}_0$, where $\overline{p}_0$ is the critical threshold, and "elastic", at constant fabric, for $p_0 > \overline{p}_0$.

More recently, Magnanimo et al. [33] have tested further the relation between microstructure and elastic moduli in isotropic granular assemblies. By using a specific numerical protocol, they succeeded to isolate three state variables and analyse their role independently, namely the pressure $p_0$, volume fraction $\phi$ and coordination number $Z$. Set of data prepared by increasing pressure and letting the coordination number free to change as well show a behaviour similar to experiments, with a relation between moduli and pressure not following the Hertzian prediction in Sect. 4.2 and dependent on the specific preparation protocol, see Fig. 5.

On the other hand, by collecting packings with similar $Z$ and fixed volume fraction $\phi$, the dependence of the elastic moduli on the confining pressure only can be analysed. Interestingly, in the case of constant structure, $G$ and $K$ both vary as $p_0^{1/3}$. That is, for packings with fixed $Z$, particles experience an increase of the contact overlap with the pressure and the behaviour of the aggregate naturally follows Hertz's law, see Fig. 6. Finally, the dependence of the elastic moduli on $Z$ is shown by plotting the bulk and shear moduli normalised by the confining pressure $p_0^{1/3}$, in Fig. 7. In this case unique curves are obtained, showing that the moduli depend on the microstructure characterised by $Z$ independently of pressure.

The findings support the micromechanical formulation of EMT. The work shows that (1) the behaviour of the elastic moduli with pressure is qualitatively recovered; (2) an independent relation of the moduli with $Z$ must be considered. However, Fig. 7 also highlights that the scaling proposed in Eqs. (31) and (30) for the moduli with $Z$ is not quantitative satisfactory. Highly coordinated packings converge to EMT with $G \sim K \sim Z^{2/3}$ and in turn converge to a constant value as expected in the "elastic" regime [47] where a very dense contact network prevents further rearrangements. Differently, data at low $Z$ strongly deviate from the EMT prediction. Thus, we conclude that more sophisticated theories, taking in account relaxation of grains, due the disordered microstructure of the packing, are needed in order to capture the material behaviour over a wide range of pressure and coordination number. Those will be treated in the following section.

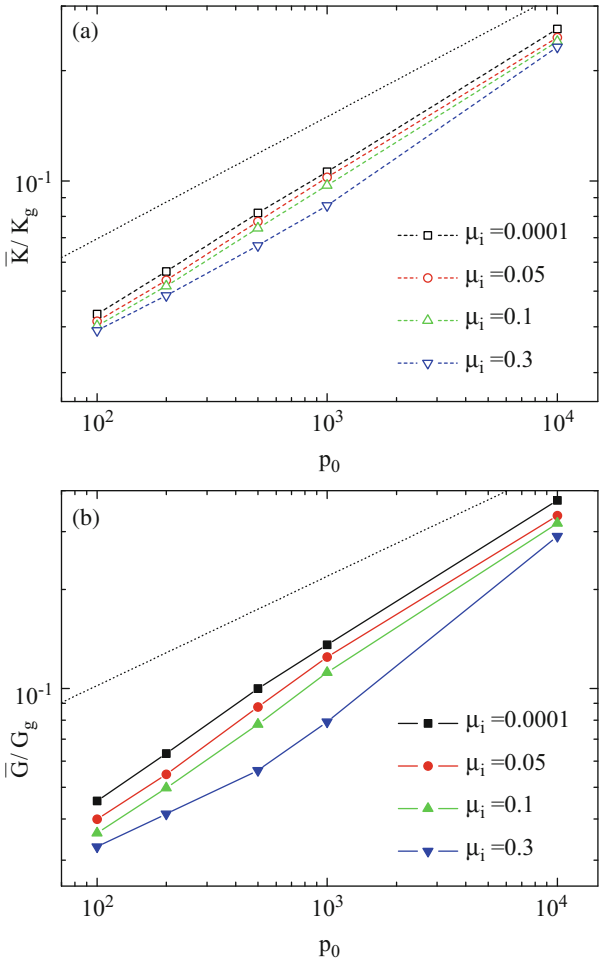


**Fig. 5** Elastic moduli $K$ and $G$, normalised by the material moduli $K_g$ and $G_g$, vs. the confining pressure $p_0$, for four groups of packings. $\mu_i$ defines the preparation protocol [33]

## 6 Micromechanical Modelling Beyond EMT

In the last 30 years, efforts have been made to improve upon the Effective Medium Theory. The so-called fluctuations theories are micromechanically based and describe the particle displacements as the sum of a fluctuation component along with the average term. Koenders [32] was the first one to introduce fluctuation about the average deformation of contacting discs. Misra and Chang [37] for the first time applied a fluctuation in strain to the calculation of the stiffness of a packing of

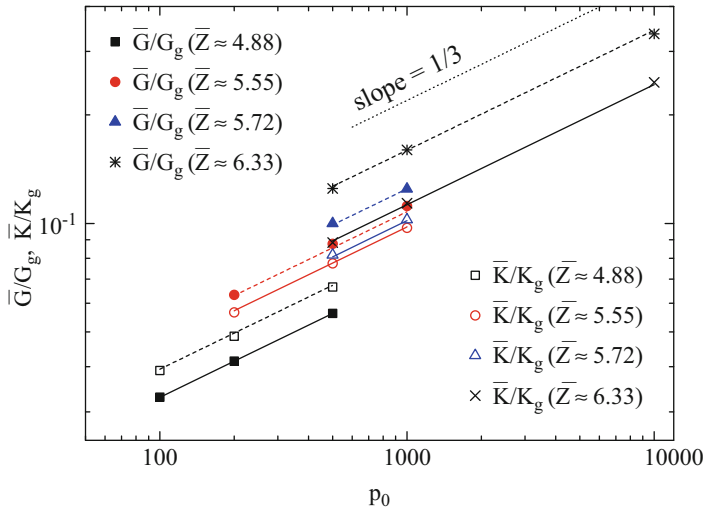


**Fig. 6** Normalised elastic moduli, vs. confining pressure $p_0$, for four groups of packings with similar coordination numbers. $G_g$ and $K_g$ are the shear and bulk moduli of the individual particles [33]

disks, with good agreement with numerical results. Later on, [21, 43] focused on a typical pair of contacting particles that interact through both the average strain and the fluctuations, assuming that the neighbouring particles moved with the average strain.

An analytical formulation for the bulk and the shear moduli based on the pair-fluctuation method has been proposed in [20, 28]. This is briefly summarised here and we refer to the articles for details.

In the pair-fluctuation approach, the kinematics of two contacting particles is given by the average deformation and fluctuations in both translations and rotations:

$$\dot{u}_i^{(BA)} = \dot{\epsilon}_{ij} l_j^c + \dot{\Delta}_j^{(BA)} - \frac{1}{2}\epsilon_{ijk}\dot{S}_j^{(BA)} l_k^c, \tag{35}$$

where $u_i^{(BA)}, l_i^c$ have been introduced in Sect. 4, $\dot{\Delta}_j^{(BA)}$ is the increment in the difference of the fluctuations in displacement of the particles and $\dot{S}_j^{(BA)}$ is the increment in the sum of the fluctuations in the rotations about their centres. As main assumption of the fluctuation theory, all the other $n$-th particles in touch with the pair $A - B$ simply move with an average deformation.

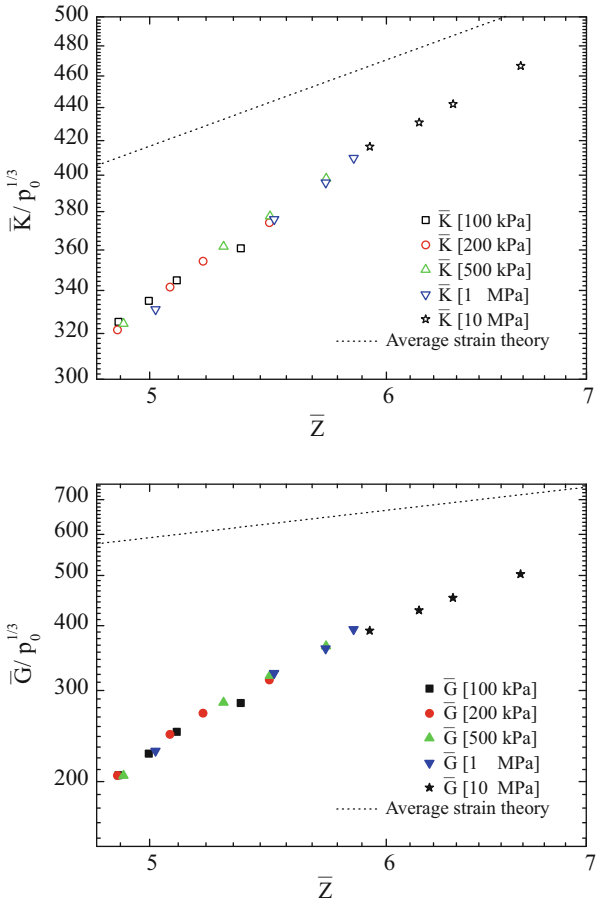


**Fig. 7** Elastic moduli K and G, normalised by $p_0^{1/3}$, vs. the coordination number $Z$: all the data collapse into unique curves [33]

After some algebra [28], and restricting our cases to $K_N/K_T \sim 1$, the expressions for the effective shear and bulk moduli proposed by EMT, Eqs. (30) and (31) are modified as follows:

$$G = \frac{6\phi}{\pi d^3}\frac{\bar{Z}d^2}{30}(K_N - K_T)(1-2\zeta) + \frac{6\phi}{\pi d^3}\frac{\bar{Z}d^2}{30}K_T\left[\frac{5}{2} - 5\zeta - 3(\xi_3 - \xi_5)\right] \tag{36}$$

and

$$K = \frac{6\phi}{\pi d^3}\frac{\bar{Z}d^2}{18}K_N(1-2\zeta), \tag{37}$$

where the coefficients $\zeta, \xi_3, \xi_5$ are functions only of the statistics of the aggregate [28], i.e., the local fabric. $\zeta, \xi_3, \xi_5$ involve the standard deviation in particle coordination number as a statistical measure of the contact geometry. In particular the coefficient is obtained from the conditional contact distribution function, which gives the probability of finding a contact at an orientation given that another contact with certain orientation is present. Along with pressure, volume fraction and coordination number, as proposed initially by EMT, the new theory states that the fluctuation in coordination number must be taken into account to characterise the contact network, and in turn, the elastic moduli.

Equations above are the solutions for the fluctuation of a typical pair of particles to be in equilibrium, assuming that the other particles in the neighbour move with the average strain. We can further improve the kinematics of a typical pair by relaxing this hypothesis. For example, in [28], the solution of the fluctuation is implemented also in the interaction of the pairs with their neighbours. In Fig. 8 we report the DEM data on bulk and shear moduli $K(Z)$ and $G(Z)$ from Fig. 7 and compare them with predictions of EMT and fluctuation theory. As shown in the figure, the pair-fluctuation theory gives an excellent prediction of the bulk modulus over a wide range of $Z$. A very good approximation is obtained for the shear modulus in the intermediate-to-high $Z$ regime, where the predicted shear modulus reduces to approximately 40% of its average strain prediction. For high coordination number EMT, fluctuation theory and DEM data converge, as highly coordinated packings of spheres tend to move according to the affine motion and the coefficients $\zeta$, $\chi_3$ and $\chi_5$ in Eqs. (36), (37) approach zero. As expected, the role of fluctuations results particularly significant for loose, low-coordinated packings. This is also confirmed by [1], where the prediction of the moduli of two-dimensional, isotropic assemblies is extended over a significant range of coordination number. The authors adopt the "particle-fluctuation" method, complementary to the "pair-fluctuation" method in [20, 28]. However, in the former, complete knowledge of the contact geometry is required, generally only available from DEM simulations.

The fluctuation theory satisfactorily improves upon EMT for the description of granular elasticity and offers interesting insights. This analysis refers to the open question on what statistical measures are needed for a comprehensive description of the microstructure. For dense systems the coordination number (and its local fluctuations) seems to be a sufficient measure of the contact geometry (Fig. 8). Simulations and theory still diverge for poorly coordinated samples, when the jamming point is approached, i.e., the transition from solid to fluid state [19]. For those systems no statistical measure may be sufficient. In [25], the authors show that, by increasing the order (or size) the sub-assemblies, the predictions get closer to the true moduli determined from DEM simulations. In turn, the full knowledge of the contact geometry is required, for a correct prediction of the material response in the isostatic limit, since a small change leads to large rearrangement of contact forces. Specific issues related to low-coordinated packings are discussed in [2]. The authors suggest that collective effects determine the rigidity properties of tenuous networks in the low-$Z$ limit, where the shear moduli vanish. In these circumstances, pair-fluctuations theory, based on the local equilibrium of one pair of grains embedded

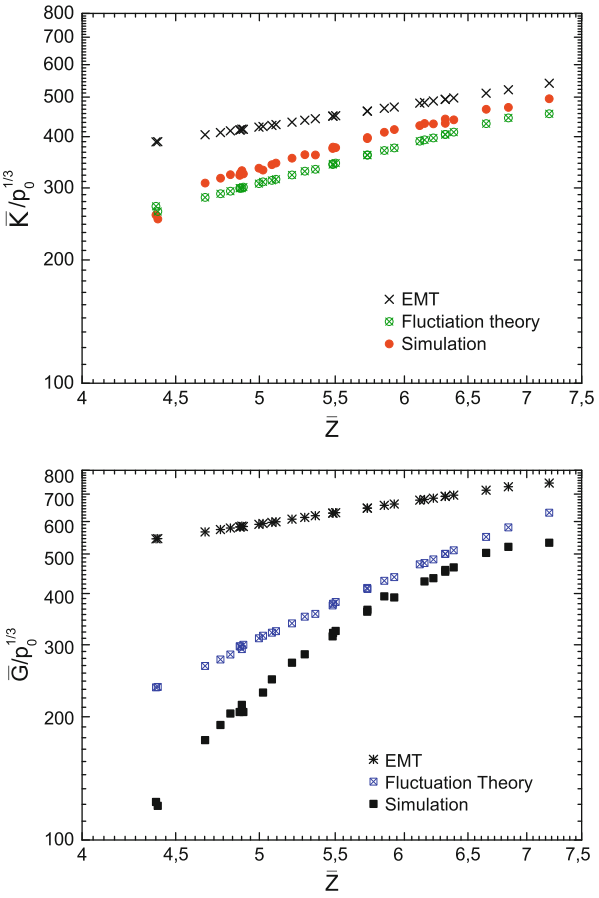


**Fig. 8** Comparison between the numerical data and fluctuation theory for the normalised (left panel) bulk modulus and (right panel) shear modulus

in an elastic medium, does not correctly represent the granular system and is thus unable to capture its behaviour.

## 7 Toward Waves in Multiphase Granular Media

In this section the Effective Medium Theory introduced in Sect. 4.2 is extended to describe the elasticity of granular media immersed in a fluid phase. In particular, the complex case of unsaturated soils is treated, and EMT is applied to predict the nonlinear behaviour of shear stiffness.

## 7.1 Micromechanical Modelling of Unsaturated Soils

For the case of small-strain stiffness of soils in unsaturated state, a number of models have recently been proposed to quantify the shear modulus $G$ over a wide range of degrees of saturation [12, 24, 36, 41, 49]. $G$ is recognised to be affected by both suction and degree of saturation, which may vary independently because of the hydraulic hysteresis and the dependency of the void ratio on the water retention behaviour. A key question is how these two variables control the small-strain stiffness and whether they can be combined into a single variable. A common approach adopted by several authors [24, 41, 49] is to derive empirical or semi-empirical relationships for $G$ using the product between suction and degree of saturation as a stress variable [22], often referred to as Bishop's effective stress for unsaturated soils:

$$\sigma''_{ij} = \sigma_{ij} - u_a \delta_{ij} + (S_r s)\delta_{ij}, \tag{38}$$

where $\sigma$ is the total stress, $u_a$ is the pore pressure, $s$ is the suction, $S_r$ is the degree of saturation and $\delta_{ij}$ is the Kronecker delta. An implicit assumption in this approach is that, at the same suction, the product $S_r s$ increases with an increase in degree of saturation. Since the degree of saturation along a drying path is higher than the degree of saturation along a wetting path, one would expect $G$ to be higher along a drying path. Although an evidence of this has been observed experimentally [23], a number of experimental investigations show an opposite trend, i.e., the soil is observed to be significantly stiffer along a wetting path [24, 40]. Inspection of experimental data also reveals that the change of $G$ with suction or degree of saturation occurs in either a monotonic or non-monotonic fashion [23, 45]. Ideally, a stiffness model should be capable of capturing the physics behind the two observed behaviours. However, no models presented so far are capable of addressing causes and differences.

A recent work [42] presents an experimental investigation of the independent effect of suction and degree of saturation on $G$ along a full hydraulic hysteresis loop. An unsaturated sand specimen was tested in a modified triaxial cell apparatus equipped with bender elements using the hanging water column method (see [42] for details on the experiments). Then, a simple macroscopic model based on micromechanical insights from EMT is proposed in order to interpret and predict the evolution of $G$ during hydraulic hysteresis. The proposed model is then challenged to elucidate a range of different responses observed in the literature.

The intergranular stress $\sigma^*_{ij}$ induced by the degree of saturation/suction may be formulated by considering an idealised packing of equal spheres in an ordered structure. Let us consider the idealised unsaturated packing as shown in Fig. 9, and let us assume that the contact area of each pair of spherical particles is a point. The two-phase material can be described as the coexistence of a region fully occupied by

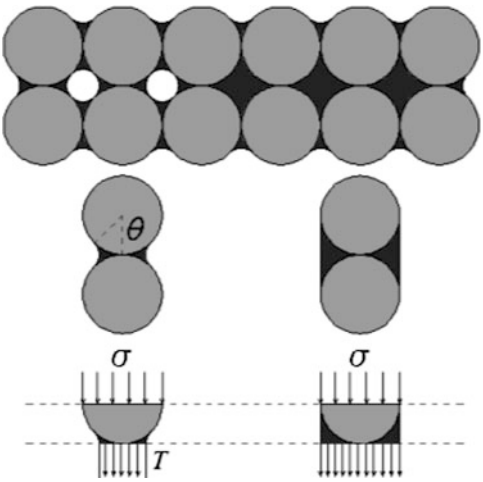


**Fig. 9** Schematic representation of the unsaturated soil packing [42]. $T$ is the surface tension at the interface between particle and water meniscus

bulk water (saturated region) and a region occupied by the menisci alone. Boso et al. [5] derived an expression of the intergranular stress $\sigma_i$ of the unsaturated packing as

$$\sigma_{ij}^{*} = \sigma_{ij} + \left[\sigma_{ij}^{*b}\frac{S_r - S_{rm}}{1 - S_{rm}} + \sigma_{ij}^{*m}\left(1 - \frac{S_r - S_{rm}}{1 - S_{rm}}\right)\right], \tag{39}$$

where $S_r$ is the total degree of saturation, $S_{rm}$ is the residual degree of saturation (degree of saturation of the region occupied by the menisci alone), $\sigma_{ij}$ is the total stress, $\sigma_{ij}^{*b}$ is the intergranular stress in the bulk water region and $\sigma_{ij}^{*m}$ is the intergranular stress in the meniscus water region. The first term in square brackets takes into account the contribution of suction to the intergranular stress in the saturated region, which is directly proportional to the suction ($\sigma_{ij}^{*b} = s$). The second term in square brackets indicates the contribution of suction to the intergranular stress in the meniscus water region. The two contributions of suction in Eq. (39) are weighed by functions of the degree of saturation.

By extending the analysis in [14] for spherical particles the stress in the menisci region $\sigma_{ij}^{*m}$ can be assumed independent of suction. As further step, we use the Effective Medium Theory in the simplified case of a regular lattice to express the shear modulus in terms of the intergranular stress. Starting from Eq. (27) applied, for example, to a Cubic Square lattice shown in Fig. 9, the shear stiffness is

$$G = C_{1212} = \frac{2}{7}\frac{d^2}{V}\frac{3}{2}k_{n0}^{2/3}\left(\frac{p_0^{*}}{2d}V\right)^{1/3}, \tag{40}$$

with $d = D_{50}$ average diameter of the particles and the volume $V$ is extended to the whole experimental sample, and only the normal component of the intergranular stress tensor has been considered $p_0^{*} = 1/3\mathrm{tr}(\sigma_{ij}^{*})$. The proposed model was calibrated and validated against the experimental results. Two model parameters

need to be identified, namely $k_{n0}$ and $p_0^{*m}$. In the macroscopic model, these parameters should be intended as macroscopic parameters with an intuitive physical micromechanical meaning. In particular, $k_{n0}$ is proportional to the interparticle stiffness $K_N$ in Sect. 4, but it is assigned an extended physical meaning. $k_{n0}$ is a model parameter that accounts for a number of characteristics of the real soil packing including the particle stiffness, particle shape, particle size distribution, particle arrangements, etc. With proper calibration, e.g., at saturation and at residual saturation, the two calibration parameters can be devised.

Figure 10 shows the comparison between the values of $G$ obtained experimentally and the simulated stiffness $C_{1212}$. In order to take into account the variability of the degree of saturation within the specimen, bounding values of $C_{1212}$ are considered, corresponding to the values of suction at the top/bottom of container. The model gives an accurate prediction of the small-strain shear modulus during hydraulic hysteresis. The variation of $G$ with suction is well captured at a qualitative and quantitative level.

Moreover, the proposed model is able to elucidate the mechanisms behind different patterns of small-strain response in unsaturated granular materials. Two key responses can be successfully reproduced: soils have been observed to exhibit a stiffer behaviour along either a drying or a wetting path; $G$ has been observed to vary in either a monotonic or non-monotonic fashion. By accounting for the independent effect of suction and degree of saturation on soil stiffness and with

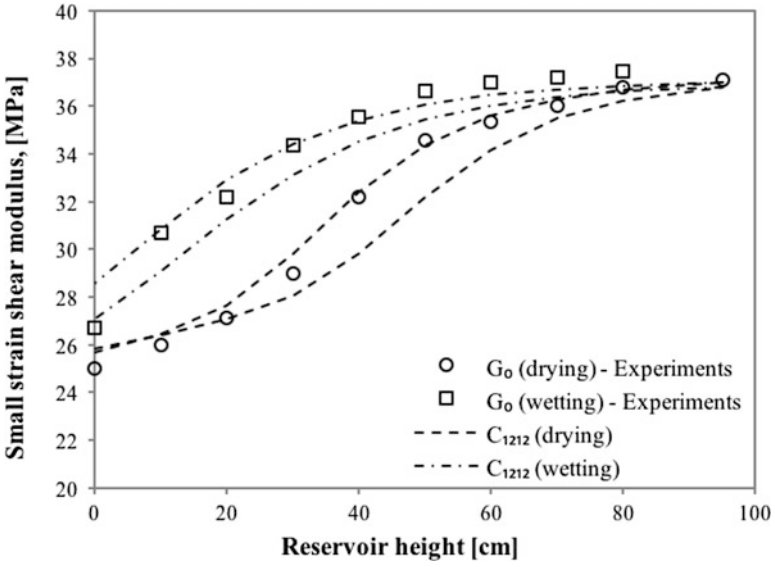


**Fig. 10** Comparison of experimental data and prediction of the micromechanical model for small-strain stiffness during hydraulic hysteresis. The two dashed lines for the drying path (dashed-dotted for the wetting path) indicate the boundaries of the theoretical prediction for the two extreme values of suction at the top/bottom of the container [42]

proper calibration of only two constants, both mechanisms can be reproduced and interpreted from the micromechanical point of view at a qualitative and quantitative level. The model captures the higher stiffness observed along a wetting path that the stress variable obtained as the product suction times degree of saturation fails to predict. According to the proposed model, the evolution of $G$ is controlled by the evolution of the intergranular stress induced by suction and degree of saturation during hydraulic hysteresis. This naturally leads to the conclusion that the breadth of the water retention curve and the intensity of the intergranular stress due to the presence of the menisci have an effect on the evolution of $G$ and control its monotonic/non-monotonic behaviour. The reader is referred to [42] for details and more extended analysis.

## 8 Conclusions

We have given an overview of the most relevant theoretical approaches to describe the elastic responses of granular soils across the geomechanical, mechanical and physics communities. Via the between experiment-based empirical models and classical micromechanical Effective Medium Theory (EMT), we have investigated the relevant parameters needed to describe the elastic response of a dense granular soil.

The study has been further enriched through insights from Discrete Element simulations. First, we have shown that waves propagating in regular arrays of particles perfectly follow the prediction of EMT. Later on, we have employed DEM to show that, in the case of random isotropic aggregates, a non-trivial dependence between pressure $p_0$, volume fraction $\phi$ and coordination number exists. In particular, for packing with identical microstructure $Z$, the elastic moduli confirm the scaling $K \sim G \sim p_0^{1/3}$ expected because of the Hertzian interaction between spheres. In addition to $p_0, \phi, Z$, we also considered the fluctuation in the number of contacts per particle and compared DEM simulations with the more sophisticated fluctuation theory that include the relaxation of grains kinematics, due to the disordered microstructure of the packing. We conclude that several regimes define the elastic behaviour of granular soils: at very high pressure (high coordination number), where contact rearrangements are impeded and the coordination number is constant, the aggregate behaves "elastically", i.e., $K \sim G \sim p_0^{1/3}$; when $p_0$ and $Z$ decrease, changes in pressure induce changes in contacts and the behaviour becomes "plastic". For sufficiently high coordination number, where movement is limited and particles tend to follow the affine motion, the prediction of EMT $K \sim G \sim Z^{2/3}$ is confirmed by DEM. For lower values of $Z$, the elastic behaviour is qualitatively but not quantitatively captured by the Effective Medium Theory. In this regime, modifications that include the local distribution of contacts succeed to improve upon EMT, with fluctuations increasing with decreasing $Z$. In the limit of poorly coordinated systems, close to jamming, fluctuation theories fail to

describe granular elasticity, and contact fluctuations must be extended from local to collective, including the whole packing of particles.

Finally, we have extended the Effective Medium framework to describe unsaturated soils and shown validation of the model against laboratory experiments after proper calibration. Experimental results revealed that wave velocity and, hence, stiffness are not controlled by the product "suction times degree of saturation", traditionally used for describing the behaviour of shear waves in unsaturated sand. According to the simplified micromechanical model the evolution of the shear modulus $G$ is controlled by the evolution of the suction-generated intergranular stress during drying-wetting cycles.

**Acknowledgments** Inspiring discussions with J.T. Jenkins, L. La Ragione, S. Luding, K. Taghizadeh Bajgirani, H. Cheng, A. Tarantino and A.G. Pagano are grateful acknowledged.

## References

1. I. Agnolin and N. P. Kruyt. On the elastic moduli of two-dimensional assemblies of disks: Relevance and modeling of fluctuations in particle displacements and rotations. *Computers and Mathematics with Applications*, 55(2):245–256, 2008.
2. I. Agnolin and J.N. Roux. Internal states of model isotropic granular packings. III. Elastic properties. *Physical Review E*, 76(6):061304, 2007.
3. K. Aki and P. Richards. *Quantitative Seismology*. Freeman, New York, 1980.
4. R. Bellotti, M. Jamiolkowski, D.C.F. LoPresti, and D.A. O'Neill. Anisotropy of small strain stiffness in Ticino sand. *Géotechnique*, 46(1):115–131, 1996.
5. M. Boso, A. Tarantino, and L. Mongioví. *Shear strength behaviour of a reconstituted clayey silt. Unsaturated soils*, pages 9–14. Taylor & Francis Group, London, 2005.
6. J.B. Burland. Ninth Laurits Bjerrum memorial lecture: "small is beautiful" - the stiffness of soils at small strains. *Canadian Geotechnical Journal*, 26(4):499–516, 1989.
7. Y.-C. Chen, I. Ishibashi, and J.T. Jenkins. Dynamic shear modulus and fabric: part I, depositional and induced anisotropy. *Géotechnique*, 38(1):25–32, 1988.
8. P.A. Cundall and O.D.L. Strack. A discrete numerical model for granular assemblies. *Géotechnique*, 29(1):47–65, 1979.
9. J. David and N. Cheeke. *Fundamentals and Applications of Ultrasonic Waves*. CRC Press, Boca Raton, 2002.
10. P.J. Digby. The effective elastic moduli of porous granular rocks. *ASME Journal of Applied Mechanics*, 48(4):803–808, 1981.
11. S.N. Domenico. Elastic properties of unconsolidated porous sand reservoirs. *Geophysics*, 42(7):1339–1368, 1977.
12. Y. Dong and N. Lu. Correlation between small-strain shear modulus and suction stress in capillary regime under zero total stress conditions. *Journal of Geotechnical and Geoenvironmental Engineering*, 142(11):4016056, 2016.
13. A. Ezaoui and H. Di Benedetto. Experimental measurements of the global anisotropic elastic behaviour of dry Hostun sand during triaxial tests, and effect of sample preparation. *Géotechnique*, 59(7):621–635, 2009.
14. R.A. Fisher. On the capillary forces in an ideal soil; correction on formulae given by W.B. Haines. *Journal of Agricultural Science*, 16(3):492–505, 1926.
15. J.D. Goddard. Nonlinear Elasticity and Pressure-Dependent Wave Speeds in Granular Media. *Proceedings of the Royal Society A*, 430(1878):105–131, 1990.

16. B.O. Hardin and W.L. Black. Elastic wave velocities in granular soils. *Journal of Soil Mechanics and Foundations Division*, 92(2):27–42, 1966.
17. B.O. Hardin and F.E.Jr Richart. Elastic wave velocities in granular soils. *Journal of Soil Mechanics and Foundations Division*, 89(1):33–66, 1963.
18. H. Hertz. Über die berührung fester elastischer körper (on the contact of elastic solids). *J. Reine und Angewandte Mathematik*, 92:156–171, 1882.
19. H.M. Jaeger, S.R. Nagel, and R.P. Behringer. Granular solids, liquids and gases. *Review Modern Physics*, 68(4):1259–1273, 1996.
20. J. Jenkins, D. Johnson, L. La Ragione, and H.A. Makse. Fluctuations and the effective moduli of an isotropic, random aggregate of identical, frictionless spheres. *Journal of the Mechanics and Physics of Solids*, 53(1):197, 2005.
21. J.T. Jenkins. *Inelastic behavior of random arrays of identical spheres*, chapter Mechanics of Granular and Porous Materials, page 11. Kluwer, Amsterdam, 1997.
22. C. Jommi. Remarks on the constitutive modelling of unsaturated soils. In *Experimental evidence and theoretical approaches in unsaturated soils*, 2000.
23. A. Khosravi. Characterizing the variation of small strain shear modulus for silt and sand during hydraulic hysteresis. In *Proceedings of the 3rd European Conference on Unsaturated Soils E-UNSAT 2016*, number 9, page 10418. A.A. Balkema Publishers, 2016.
24. A. Khosravi and J.S. McCartney. Resonant column test for unsaturated soils with suction-saturation control. *Geotechnical Testing Journal*, 36(6):1–10, 2011.
25. N.P. Kruyt, I. Agnolin, S. Luding, and L. Rothenburg. Micromechanical study of elastic moduli of loose granular materials. *Journal of the Mechanics and Physics of Solids*, 58(9):1286–1301, 2010.
26. N.P. Kruyt and L. Rothemburg. Micromechanical definition of the strain tensor for granular materials. *Journal of Applied Mechanics*, 63(3):706–711, 1996.
27. R. Kuwano and Jardine R.J. On the applicability of cross-anisotropic elasticity to granular materials at very small strains. *Géotechnique*, 52(10):727–749, 2002.
28. L. La Ragione and J. Jenkins. The initial response of an idealized granular material. *Proceedings of the Royal Society A*, 463(2079):735–758, 2007.
29. J.-S. Lee and J.C. Santamarina. Bender elements: Performance and signal interpretation. *Journal of Geotechnical and Geoenvironmental Engineering*, 131(9):1063–1070, 2005.
30. D.C.F. LoPresti, M. Jamiolkowski, O. Pallara, A. Cavallaro, and S. Pedroni. Shear modulus and damping of soils. *Géotechnique*, 47(3):603–617, 1997.
31. A.E.H. Love. *A Treatise on the Mathematical Theory of Elasticity*. Cambridge University Press, Cambridge, 1927.
32. Koenders M.A. The incremental stiffness of an assembly of particles. *Acta Mechanica*, 70(1–4):31–49, 1987.
33. V. Magnanimo, L.L. La Ragione, J.T. T. Jenkins, P. Wang, and H.A.A. Makse. Characterizing the shear and bulk moduli of an idealized granular material. *Europhysics Letters*, 81(3):34006, 2008.
34. R.J. Mair. Developments in geotechnical engineering research: Application to tunnels and deep excavations. volume 97 of *Proceedings of the Institution of Civil Engineers-Civil Engineering*, pages 27–41. Thomas Telford-ICE Virtual Library, 1993.
35. H.A. Makse, N. Gland, D.L. Johnson, and L. Schwartz. Why effective medium theory fails in granular materials. *Physical Review Letters*, 83:5070, 1999.
36. C. Mancuso, R. Vassallo, and A. d'Onofrio. Small strain behaviour of a silty sand in controlled-suction resonant column-torsional shear tests. *Canadian Geotechnical Journal*, 39(1):22–31, 2002.
37. A. Misra and C.S. Chang. Effective elastic moduli of heterogeneous granular solids. *International Journal of Solids and Structures*, 30(18):2547–2566, 1993.
38. O. Mouraille, W.A. Mulder, and S. Luding. Sound wave acceleration in granular materials. *Journal of Statistical Mechanics: Theory and Experiments*, 2006(07):P07023, 2006.
39. D. Muir Wood. Life cycles of granular materials. *Philosophical Transactions of Royal Society London A*, 356(1747):2453–2470, 1998.

40. C.W.W. Ng and J. Xu. Effects of current suction ratio and recent suction history on small-strain behaviour of an unsaturated soil. *Canadian Geotechnical Journal*, 49(2):226–243, 2012.
41. W.T. Oh and S.K. Vanapalli. Semi-empirical model for estimating the small-strain shear modulus of unsaturated non-plastic sandy soils. *Geotechnical and Geological Engineering*, 32(2):259–271, 2014.
42. A. Pagano, A. Tarantino, and V. Magnanimo. A microscale-based model for small-strain stiffness in unsaturated granular geomaterials. *Géotechnique*, 69(8):687–700, 2019.
43. A.C. Paine. Calculation of the effective moduli of a random packing of spheres using a perturbation of the uniform strain approximation. In *Proceedings of Powders and Grains 1997*, 1997.
44. P. Philippe and D. Bideau. Compaction dynamics of a granular medium under vertical tapping. *Europhysics Letters*, 60(5):677, 2002.
45. X. Qian, D.H. Gray, and R.D. Woods. Voids and granulometry: effects on shear modulus of unsaturated sands. *Journal of Geotechnical Engineering*, 119(2):295–314, 1993.
46. S.K. Roesler. Anisotropic shear modulus due to stress anisotropy. *Journal of Geotechnical Engineering*, 105(7):871–880, 1979.
47. J.C. Santamarina. *Soils and waves: particulate materials behavior, characterization and process monitoring*. Wiley, 2001.
48. J.C. Santamarina and Cascante G. Stress anisotropy and wave propagation: a micromechanical view. *Canadian Geotechnical Journal*, 33(5):770–782, 1996.
49. A. Sawangsuriya, T.B. Edil, and P.J. Bosscher. *Journal of Geotechnical and Geoenvironmental Engineering*, 135(10):1390–1403, 2009.
50. E. Somfai, J.N. Roux, J.H. Snoeijer, M. van Hecke, and W. van Saarloos. Elastic wave propagation in confined granular systems. *Physical Review E*, 72(2):021301, 2005.
51. C. Thornton. Numerical simulations of deviatoric shear deformation of granular media. *Géotechnique*, 50(1):43–53, 2000.
52. K. Walton. The effective elastic moduli of a random packing of spheres. *Journal of Mechanics and Physics of Solids*, 35(2):213–226, 1987.